Supplement of The Cryosphere, 20, 2417–2437, 2026
https://doi.org/10.5194/tc-20-2417-2026-supplement

The Cryosphere Open Access EGU

Supplement of

Analysis of long-term dynamic changes of subglacial lakes in the Recovery Ice Stream, Antarctica

Tiantian Feng et al.

Correspondence to: Tong Hao (tonghao@tongji.edu.cn)

S1. Volume change uncertainty

The uncertainty in the estimated subglacial lake volume change consists of two components: the uncertainty in lake-induced surface elevation change and the uncertainty in lake area. We compute the uncertainty in lake-induced surface elevation change following a two-step error propagation procedure. First, we calculate the uncertainty in ice surface elevation change. This uncertainty includes the altimetry measurement error, σ_H (0.15 m for ICESat (Zwally et al., 2012); 0.09 m for ICESat-2 (Brunt et al., 2019)), and the DEM interpolation uncertainty σ_{dem} derived using the Monte Carlo method (Siegfried et al., 2014). The resulting uncertainty σ in ice surface elevation change is calculated in Equation S1:

$$\sigma = \sqrt{\sigma_H^2 + \sigma_{dem}^2}. \tag{S1}$$

Next, we compute the uncertainty in lake-induced surface elevation change. As described in Equation 1 of the main text, lake-induced surface elevation change is obtained from the difference between the interior and exterior elevation change signals, which removes the regional ice dynamic background trend. The uncertainty of interior and exterior elevation change can be calculated by using Equation S1. Then, error propagation yields the uncertainty in lake-induced surface elevation change for a specific observation period, $\sigma_{\Delta h}$, as given by Equation S2:

$$\sigma_{\Delta h} = \sigma \cdot \sqrt{\frac{\sum_{i=1}^{N_{\text{in}}} p_i^2}{\left(\sum_{i=1}^{N_{\text{in}}} p_i\right)^2} + \frac{\sum_{j=1}^{N_{\text{out}}} p_j^2}{\left(\sum_{j=1}^{N_{\text{out}}} p_j\right)^2}}, \tag{S2}$$

where N_{in}, N_{out} denote the quantities of lake interior and exterior points respectively. p_i, p_j correspond to the weights, which are assigned based on the minimum distance from the elevation measurement points to the lake outline, and are normalized to sum to 1 for the interior and exterior points separately.

The lake outlines are delineated based on multi-temporal surface elevation anomalies, which inevitably introduces area estimation uncertainty; accordingly, we adopt a 10% area estimation error following Kim et al. (2016). Combining the lake area uncertainty with the elevation change uncertainty yields the final uncertainty of lake volume change.

Given that the distribution of measurement points and the elevation changes vary across different lakes and observation periods, we calculate the average volume change uncertainties over different observation periods for each lake to facilitate quantitative analysis. Specifically, for ICESat-2 mission period, we compute the monthly average uncertainties; for ICESat mission period, we calculate the average uncertainties for each campaign. The resulting volume change uncertainties are presented in Table S1.

Table S1. Volume change uncertainties of active subglacial lakes in the RIS region during ICESat and ICESat-2 missions.

Lake Name	σ *(m)*		$\sigma_{\Delta h}$ *(m)*		*Volume uncertainty (km^3)*	
	ICESat	*ICESat-2*	*ICESat*	*ICESat-2*	*ICESat*	*ICESat-2*
Rec1-1	*3.20*	*3.20*	*0.48*	*0.04*	*0.06*	*0.01*
Rec1-2	*0.84*	*0.83*	*0.07*	*0.01*	*0.10*	*0.01*
Rec2	*1.99*	*1.99*	*0.15*	*0.01*	*0.09*	*0.02*
Rec3	*0.60*	*0.59*	*0.08*	*0.01*	*0.01*	*0.00*
Rec4	*0.38*	*0.36*	*0.04*	*0.00*	*0.03*	*0.01*
Rec5	*0.32*	*0.30*	*0.03*	*0.00*	*0.02*	*0.00*
Rec6-1	*1.45*	*1.44*	*0.13*	*0.01*	*0.14*	*0.02*
Rec6-2	*2.88*	*2.88*	*0.54*	*0.05*	*0.04*	*0.00*
Rec7	*0.24*	*0.21*	*0.03*	*0.00*	*0.01*	*0.00*
Rec8	*0.17*	*0.12*	*0.01*	*0.00*	*0.03*	*0.00*
Rec9	*0.20*	*0.16*	*0.02*	*0.00*	*0.01*	*0.00*
RecN1	*0.92*	*0.92*	*0.14*	*0.01*	*0.02*	*0.00*
RecN2	*1.96*	*1.96*	*0.03*	*0.02*	*0.01*	*0.01*
RecN3	*0.53*	*0.52*	*0.08*	*0.01*	*0.01*	*0.00*
RecN4	*1.01*	*1.00*	*0.05*	*0.02*	*0.03*	*0.00*
RecN5	*0.63*	*0.62*	*0.06*	*0.01*	*0.05*	*0.00*
RecN6	*0.27*	*0.25*	*0.04*	*0.00*	*0.01*	*0.00*
RecN7	*0.32*	*0.30*	*0.08*	*0.01*	*0.04*	*0.00*
RecN8	*0.47*	*0.45*	*0.07*	*0.01*	*0.01*	*0.00*
RecN9	*0.27*	*0.24*	*0.04*	*0.00*	*0.01*	*0.01*
RecN10	*0.32*	*0.30*	*0.13*	*0.00*	*0.08*	*0.01*
RecN11	*0.29*	*0.26*	*0.08*	*0.00*	*0.05*	*0.00*
RecN12	*0.52*	*0.50*	*0.09*	*0.00*	*0.02*	*0.01*
RecN13	*0.35*	*0.33*	*0.10*	*0.00*	*0.01*	*0.00*
RecN14	*0.27*	*0.24*	*0.02*	*0.00*	*0.01*	*0.00*

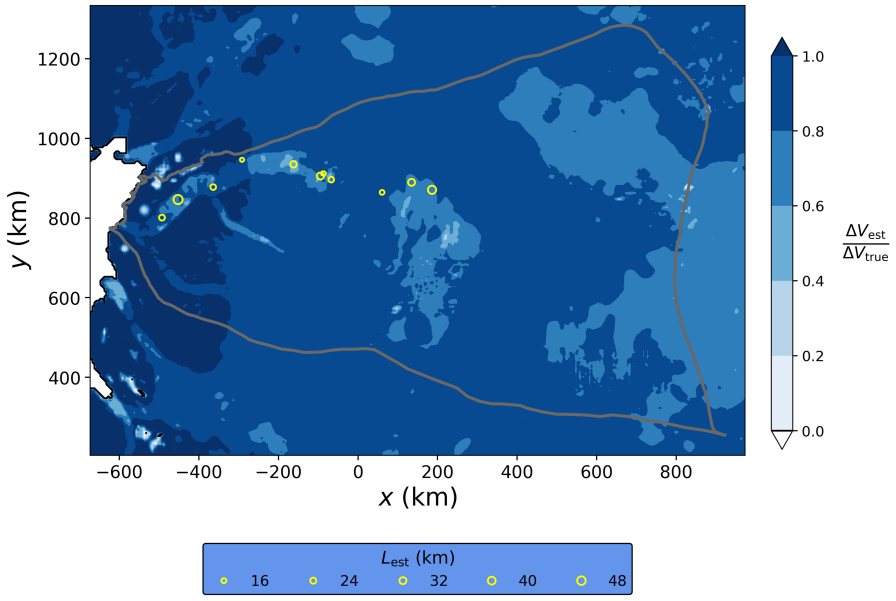

Figure S1. Spatial distribution of the volume change ratio ($\frac{\Delta V_{\text{est}}}{\Delta V_{\text{true}}}$) for subglacial lakes on the RIS, derived from the model framework of Stubblefield et al. (2021) for a 3-year filling-draining cycle period. Active subglacial lakes along the primary drainage pathways are indicated by yellow circles positioned at the centroid of each lake's minimum bounding rectangle, with circle size scaled by the rectangle's longest side (L_{est}), based on updated lake outlines from this study.

Table S2. Volume change ratios ($\frac{\Delta V_{\text{est}}}{\Delta V_{\text{true}}}$) of active subglacial lakes along the primary drainage pathways in the RIS region for a 3-year filling-draining cycle period.

Lake Name	$\frac{\Delta V_{\text{est}}}{\Delta V_{\text{true}}}$
RecN10	*0.69*
Rec9	*0.79*
RecN9	*0.83*
RecN6	*0.68*
Rec6-2	*0.67*
Rec6-1	*0.74*
Rec4	*0.53*
RecN4	*0.93*
RecN2	*0.86*
Rec1-2	*0.76*
RecN1	*0.88*

S2. Annual elevation changes of subglacial lakes

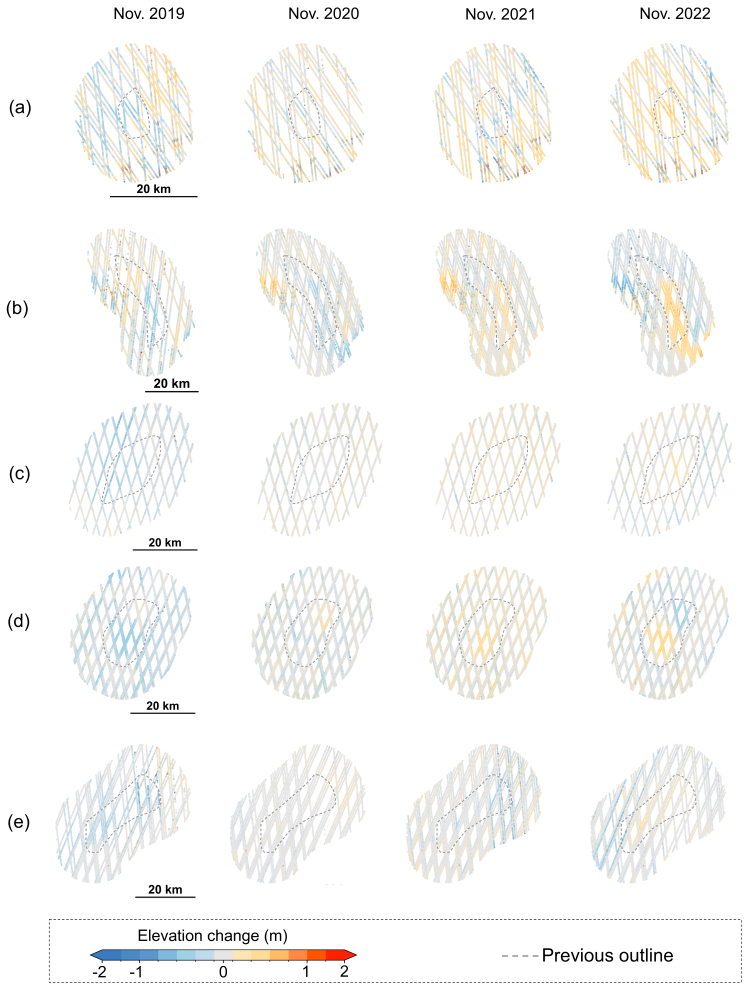

Figure S2. Previous outlines and annual elevation changes of lakes with no observed elevation changes: (a) Rec3, (b) Rec5, (c) Rec7, (d) Rec8, and (e) Rec9.

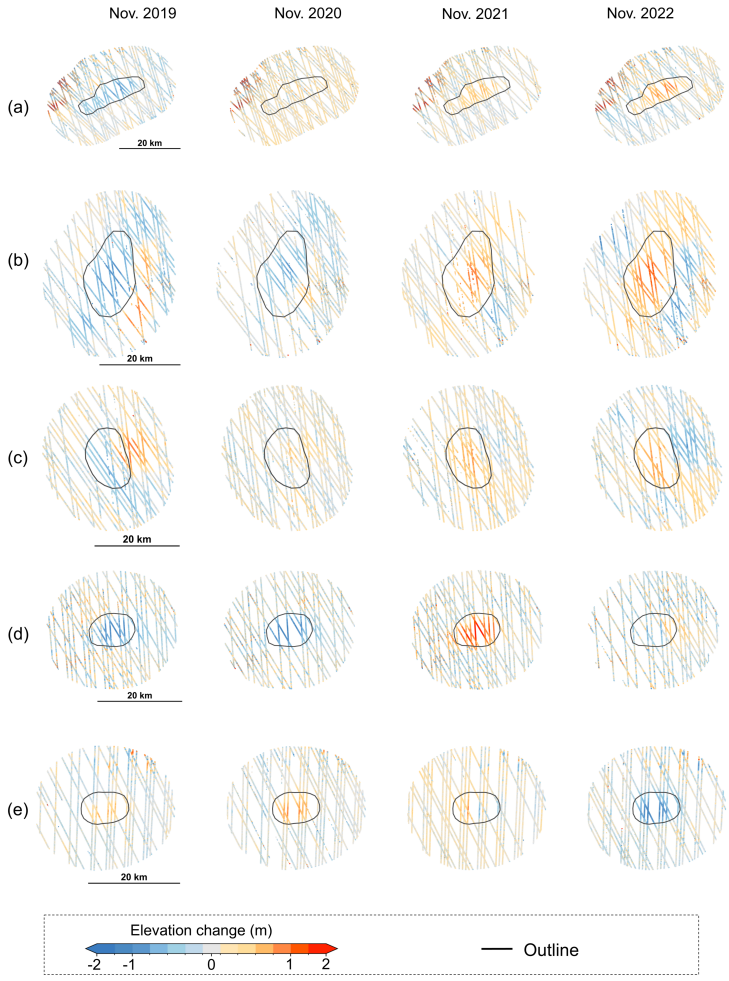

Figure S3. Outlines and the annual elevation changes of the newly identified lakes (a) RecN1, (b) RecN2, (c) RecN3, (d) RecN4, and (e) RecN5.

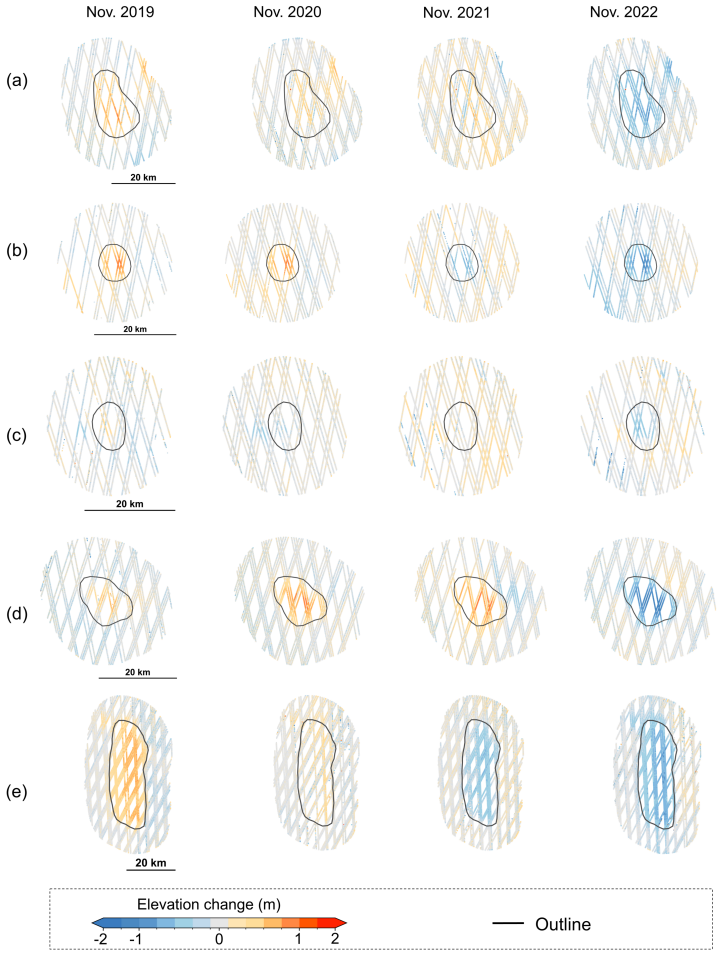

Figure S4. Outlines and the annual elevation changes of the newly identified lakes (a) RecN6, (b) RecN7, (c) RecN8, (d) RecN9, and (e) RecN10.

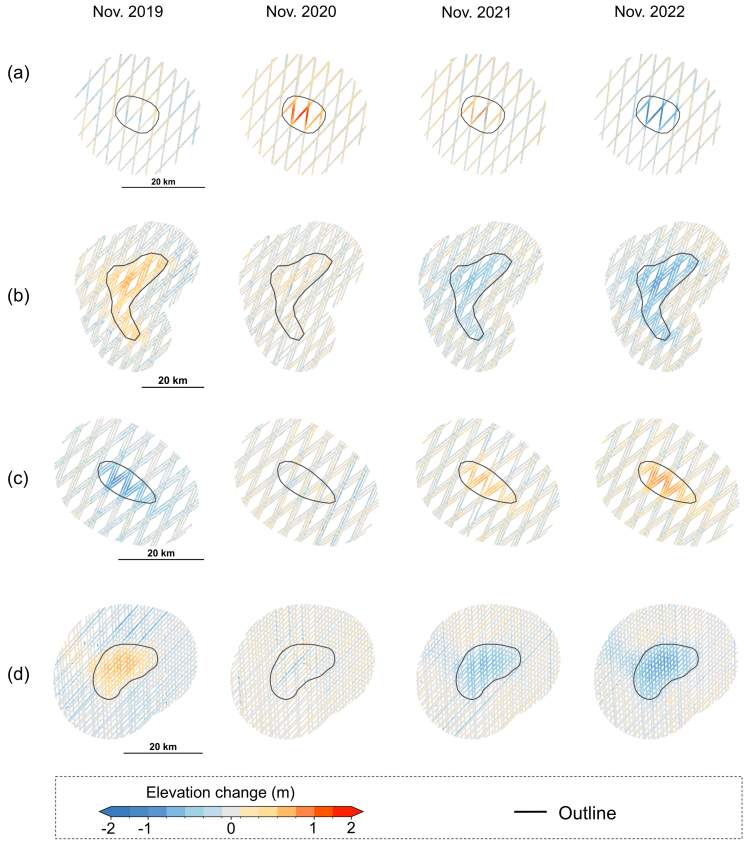

Figure S5. Outlines and the annual elevation changes of the newly identified lakes (a) RecN11, (b) RecN12, (c) RecN13, and (d) RecN14.

S3. Cascading dynamics of lakes along the primary drainage pathways

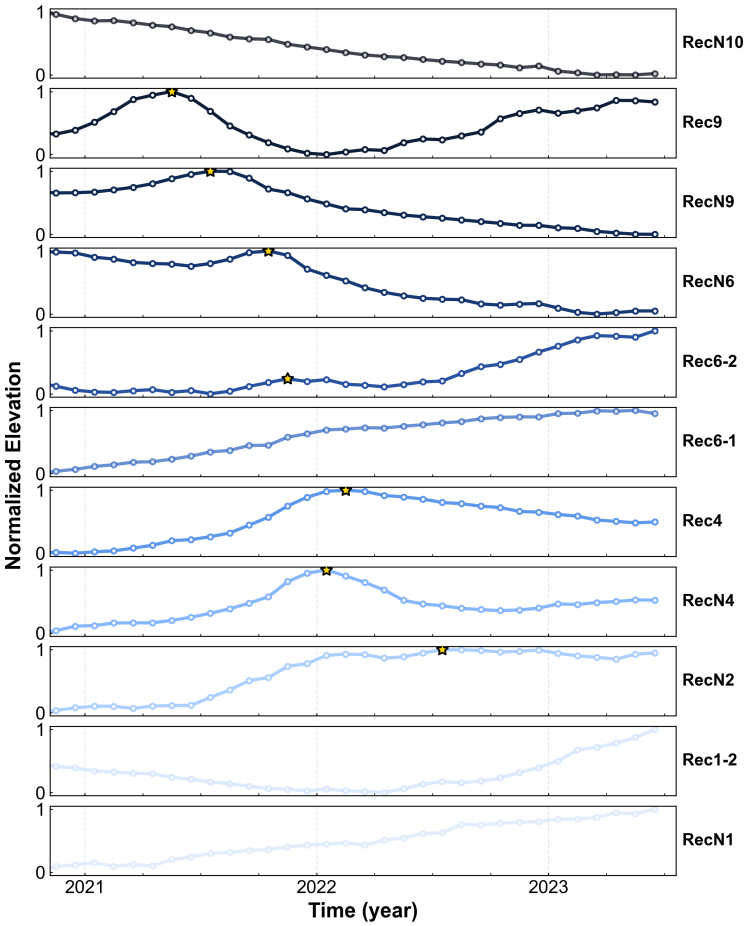

Figure S6. Normalized elevation changes and drainage onset times for lakes along the primary drainage pathway from early 2021 to mid-2023. Yellow stars indicate the drainage onset time for each lake. Elevation changes are normalized over the entire observation period for visualization purposes. The subplots are arranged from top to bottom following the upstream-to-downstream sequence of the lakes along the drainage pathway. The uppermost lake (RecN10) shows drainage initiation in June 2019, while the two lowermost lakes (RecN1 and Rec1-2) show no drainage initiation by the end of the observation period; no clear transition point is identified for Rec6-1.

References

Brunt, K., Neumann, T., and Smith, B.: Assessment of ICESat-2 ice sheet surface heights, based on comparisons over the interior of the Antarctic ice sheet, Geophysical Research Letters, 46, 13 072–13 078, https://doi.org/10.1029/2019gl084886, 2019.

Kim, B.-H., Lee, C.-K., Seo, K.-W., Lee, W. S., and Scambos, T.: Active subglacial lakes and channelized water flow beneath the Kamb Ice Stream, The Cryosphere, 10, 2971–2980, https://doi.org/10.5194/tc-10-2971-2016, 2016.

Siegfried, M. R., Fricker, H. A., Roberts, M., Scambos, T. A., and Tulaczyk, S.: A decade of West Antarctic subglacial lake interactions from combined ICESat and CryoSat-2 altimetry, Geophysical Research Letters, 41, 891–898, https://doi.org/10.1002/2013gl058616, 2014.

Zwally, H., Schutz, R., Hancock, D., and Dimarzio, J.: GLAS/ICESat L2 Antarctic and Greenland Ice Sheet Altimetry Data (HDF5), Version 33, https://doi.org/10.5067/ICESAT/GLAS/DATA205, 2012.